NUMERICAL STUDY ON THE LATERAL IMPACT RESPONSE OF PCFST COLUMNS UNDER AXIAL LOAD

A. Z. ZHU, J. W. LI, W. XU
School of Civil Engineering and Mechanics, Huazhong University of Science and Technology, Wuhan, P.R. China.
Email: zhuaizhu1228@hust.edu.cn

Abstract: In this work, a numerical study was conducted to investigate the impact response of rectangular partially concrete-filled steel tubular (PCFST) columns. A finite element analysis (FEA) model was developed, and the static axial and dynamic lateral impact loads were simultaneously considered in the column during the impact process. Parameter analysis related to several structural and load parameters was carried out. The structural parameters included the concrete-filling ratio (α_c), width–thickness ratio of steel tube (R) and concrete compressive strength. The load parameters included the impact mass (m), impact angle (θ) and axial compression ratio (μ). The impact responses, including the deformation mode, maximum displacement and impact force, were analysed. The critical impact velocity (v_{cr}), which was used to define failure in the PCFST columns, was also analysed to compare the anti-impact performance of different columns. Numerical results show that ratios α_c and R significantly influenced the anti-impact performance of the PCFST columns. The concrete compressive strength exhibited an insignificant influence on the anti-impact performance. θ and μ also significantly affected the velocity v_{cr}. v_{cr} slightly decreased with the increased impact mass m.

Keywords: Partially concrete-filled steel tubular columns, Lateral impact response, Axial load, Numerical study.

1. Introduction

Steel piers feature good application prospects in urban traffic due to their light weight, high strength, short construction period, good ductility and durability. With the development of urban traffic, vehicle collision became one of the main reasons causing the failure of bridge piers (Sharma H. et al, 2012). Bridges may be destroyed in serious vehicle–bridge collisions due to the defects of anti-impact device and design. Partially filling concrete into hollow steel columns could delay local buckling and is expected to improve the local anti-impact behaviour of steel columns. Ge et al. (1996) and Yuan et al. (2013) investigated the seismic behaviour of PCFST members. Usami et al. (1997) performed cyclic and dynamic loads on PCFST bridge piers and discovered the desirable earthquake-resistance characteristics of PCFST columns. Given that the actual columns are usually subjected to axial pressure, the axial load has been considered in relative investigations on impact responses of reinforced concrete column (Zhang R.K., 2010; Abdelkarim O.I. et al, 2017; Cai J et al, 2018). Wang et al. (2008) investigated the behaviour of CFST columns under lateral load. Their results showed that axial pressure considerably influenced the impact resistance of CFST columns. Wang et al. (2018) also studied the behaviour of concrete-filled circular steel tubular columns subjected to lateral impact loads

Proceedings of the 17th International Symposium on Tubular Structures.
Editors: X.D. Qian and Y.S. Choo

Published by Research Publishing, Singapore.
ISBN: 978-981-11-0745-0; doi:10.3850/978-981-11-0745-0_053-cd

under different axial pressures by drop-hammer experiments. The results showed that the critical fracture energy increased with the increase in axial load level under certain conditions. However, investigations on the behaviour of PCFST columns subjected to lateral impact and axial loads are unavailable. The influences of parameters on the anti-impact behaviour of PCFST columns under impact loads remain unknown.

This work aimed to study the behaviour of PCFST members under static axial and dynamic lateral impact loads. Firstly, finite element models were established using ABAQUS to simulate vehicle–pier collisions. Secondly, the critical impact velocity (v_{cr}), which was applied to define failure in the PCFST columns, was analysed. Thirdly, parameter analysis was carried out to further study the impact response of PCFST columns. Parameters, including the concrete-filling ratio (α_c), width–thickness ratio of steel tube (R) , concrete compressive strength (f_{cu}), impact mass (m), impact angle (θ) and axial compression ratio (μ), were considered. The dynamic responses, including the impact force, deformation mode and displacement response, were analysed under the impact load.

2. Finite element model

Static axial load was applied during the impact process on the basis of the finite element analysis (FEA) model verified by the authors in a previous experimental study (Zhu A.Z. et al, 2018). The material properties under impact load, boundary conditions and contact between the steel tube and infilling concrete were considered. Details of the FEA models are shown in the following sections.

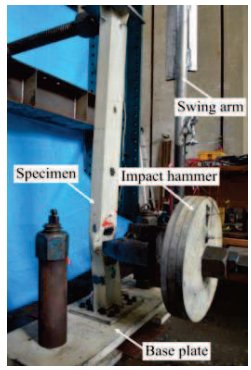

Figure 1. Test set-up[11]

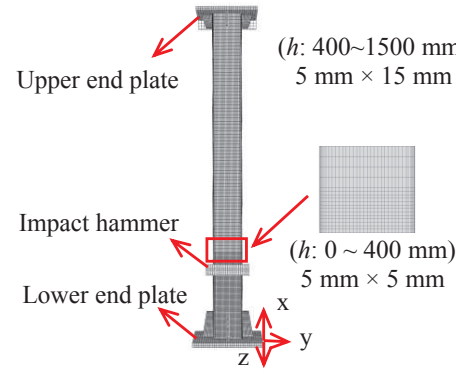

Figure 2. FEA model under lateral impact

2.1. Element mesh

Figure 2 shows the cross-section of a rectangular steel tube. The sectional dimensions of the rectangular steel tubes were 140 × 80 × 3 mm^3. The inner radius of the cold-formed corner was 4.5 mm. The total length of columns was 1500 mm. The impact centre height was 320 mm from the bottom. The steel tube was partially filled with concrete. The steel tube and infilling concrete were simulated using 4-node shell element with reduced integration and 8-node brick element with reduced integration, respectively. A mesh convergence study was carried out to determine the appropriate mesh density. Figure 2 also displays the selected element mesh for the PCFST columns. A stiffness-type hourglass control was used to eliminate the zero energy modes, and the hourglass energy was less than 5% of the total impact energy.

2.2. Materials

A stress–strain model for cold-formed steel with a multilinear isotropic strain hardening rule (Abdel-Rahman N. et al, 1997) was used to simulate the steel tube material. The cross-sections of the rectangular steel tube were divided into flat and corner zones. Different stress–strain relationships were observed for the flat and corner zones of the cold-formed sections. The yield strength and ultimate strength of the flat zones were obtained by conducting steel tensile coupon test (Zhu A.Z. et al, 2018). The yield strength of the corner zones were considered based on an empirical equation developed by Abdel-Rahman et al (1997). The ultimate tensile strength of the corner zones was calculated using Equation proposed by Tao et al (2013). Cowper–Symonds power (Han L.H. et al, 2007) was introduced to consider the effect of strain rate ($\dot{\varepsilon}$) with a multiplier factor (D) of 40.4s^{-1} and exponent (p) of 5 to achieve the dynamic yield strength.

The concrete damage plasticity (CDP) model in ABAQUS was adopted in the FEA model to simulate concrete behaviour. In the CDP model, dilation angle, flow potential eccentricity, ratio of the second stress invariant on the tensile meridian to that on compressive meridian and ratio of the compressive strength under biaxial loading to uniaxial compressive strength were set at 30°, 0.1, 2/3 and 1.16 (Tao Z. et al, 2013), respectively. The stress–strain relationship of core concrete presented by Han et al. (2007) was used to consider the increase in the plasticity behaviour of infilling concrete due to passive confinement of the steel tube. The characteristic static compressive strength of concrete was multiplied by a dynamic increase factor (1.25) to consider the effect of impact load (Mays G.C. et al, 1995).

2.3. Boundary conditions and contact

The freedoms of the bottom end plate were all restricted to realise a fixed boundary condition. The boundary conditions were assigned parallel to the z-axis of the top end plate to translate the columns in the vertical direction only. A surface-based interaction with a contact pressure model in the normal direction and a Coulomb friction model in the tangential direction was used to simulate the contact between steel and infilling concrete. The friction factor of the Coulomb friction model was 0.47 (Baltay P. et al, 1990).

2.4. Static axial load

Lateral impact load was applied in ABAQUS/Explicit dynamic analysis. A quasi-static method was adopted in this work to apply static axial pressure in ABAQUS/Explicit. In view of the stress wave generated by rapid axial loading, which would lead to structural oscillation and inaccurate results, a smooth step amplitude curve was used to apply the axial compression load (Xu W., 2019). Setting a reasonable loading time was necessary to reduce structural oscillation during quasi-static axial loading. A trial calculation was conducted to select a reasonable loading time and ensure that the axial load could maintain stability after loading. No evident fluctuation was observed in the internal stress of the structure. The kinetic energy of the structure under axial loading should not exceed 10% of the total strain energy (Hibbitt K., 2010).

2.5. Dynamic lateral impact load

After the axial compression load reached, the lateral impact load was applied. The pendulum hammer was simplified to a rigid shell surface with an initial impact velocity (v_0) and mass to simulate the vehicle impact. The rigid shell surface exhibited a 200 × 50 mm^2 dimension, consistent with the front face of the pendulum hammer. A space between the rigid shell surface and external surface of the impacted columns was reserved to apply a lateral impact load after axial loading time (Hibbitt K., 2010).

3. Parameter analysis

3.1. Definition of parameters and responses

Parameter analysis related to structural and load parameters was carried out to study the impact response of PCFST columns (Tables 1 and 2). The structural parameters comprised the concrete-filling ratio (α_c), width–thickness ratio of steel tube (R) and concrete compressive strength (f_{cu}), where $\alpha_c = h_c/h$ (h_c is the height of infilling concrete, and h is the column height), and $R = W_c/t_c$ (W_c and t_c denote the width of the column cross-section and thickness of the steel tube, respectively). The load parameters included impact mass (m), impact angle (θ) and axial compression ratio (μ), where θ indicates the angle between the impact direction and short edge of the cross-section.

The impact responses, including the deformation mode, maximum displacement and impact force, were analysed. A previous experimental study reported that the deformation modes of columns under impact load included global flexural deformation and local buckling. Failure may occur under the combined action of the lateral impact and axial compression loads. In this section, 'G' (global flexural deformation), 'L' (local buckling) and 'G + L' (global bending and local buckling) were used to represent the different deformation modes of the columns. Variable 'F' (failure) was used to denote the failure of components due to deformation. During the impact process, the rigid surface remained in contact with the impacted corner of the columns, and their displacement responses at the impacted position were similar. Therefore, the displacement response and maximum displacement (Δ_{max}) of the impacted point were selected for analysis.

At high initial impact velocity, the column would experience evident local buckling and global flexural deformation, and the axial bearing capacity of the column would drastically decrease. Under the combined action of the axial compression and lateral impact loads, the column would lose stability. The minimum impact velocity causing column failure was defined as the critical impact velocity v_{cr} (Al-Thairy H. et al, 2011). Considering model M8 (Table 1) as an example, the different responses under different initial impact velocity were obtained (Figure 3). The specific differences were as follows: (1) When the impact velocity (v_0 = 4.0 m/s) was lower than v_{cr} (v_{cr} = 5.35 m/s), the deformation modes were dominated by global flexural deformation and local buckling. When the displacement reached Δ_{max}, the velocities of the impactor and column reached zero, whereas the kinetic energy of the system decreased to the same value. With the release of elastic energy, the column rebounded together with the impactor, and the displacement decreased. (2) When the impact velocity (v_0 = 5.3 m/s) approached v_{cr} (v_{cr}= 5.35 m/s), the deformation modes were dominated by global flexural deformation and local buckling. After the maximum displacement was reached, the column slightly rebounded, and the residual kinetic energy of the system was almost equal to zero. (3) When the impact velocities (v_0 = 5.4, 6.0 m/s) were higher than v_{cr} (v_{cr}= 5.35 m/s), the column firstly experienced substantial global flexural deformation and local buckling. The impact force then decreased with the continuous and rapid increase in deformation, displacement and kinetic energy under the action of axial compression load. Finally, the column lost stability.

The above-mentioned analysis showed that whether the impact velocity reaches v_{cr} or not considerably influences the deformation mode, displacement response, impact force and kinetic energy of the system. The critical impact velocity could be used to evaluate the anti-impact performance of columns. Two velocities (v_0= 5.3, 5.4 m/s) near v_{cr} were obtained by setting different impact velocities during the model calculation to achieve v_{cr}. Therefore, the average value of the two velocities could be considered as v_{cr} (e.g. v_{cr}= 5.35 m/s) with an accuracy 0.05 m/s (0.05 m/s = 5.35 m/s × 1%).

(a) Deformation modes

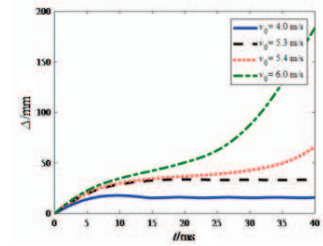

(b) Displacement versus time curve

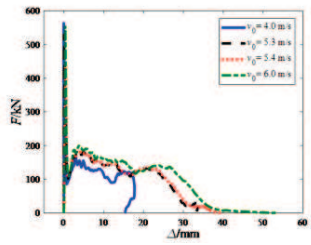

(c) Impact force versus displacement time curve

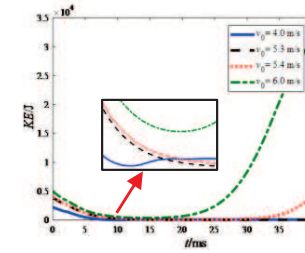

(d) Global kinetic energy time curve

Figure 3. Dynamic response of columns under different impact velocities

3.2. Analysis of structural parameters

The parameters α_c, R and f_{cu} were analysed. Table 1 shows the parameter settings and numerical results. Except for models M1–M5, the concrete-filling height of models M6–M15 was 700 mm, which was calculated from the minimum concrete-filling height equations recommended in the Japanese Code (2012). Other data of models M1–M15 were as follows: cross-section size $w_0 \times d_0$ = 140 mm × 80 mm, column height h = 1500 mm, steel strength f_y = 345 MPa, impact velocity v_0 = 4 m/s, impact mass m = 270 kg, impact angle θ = 90° and axial compression ratio μ = 0.3. Axial load was applied to the top end plate in the form of uniform force.

3.2.1 Concrete-filling rate (α_c)

The influence of α_c on impact responses was analysed by changing the concrete-filling height from 0 mm to 1500 mm at 375 mm intervals. Figures 4 (a) show the effect of α_c on the impact force–displacement (F–Δ) curve. From Figure 4 (a) and table 1, Δ_{max} decreased with the increasing α_c. The impact force of the hollow steel tubular column (model M1) was evidently lower than that of PCFST columns. Partially filling concrete could effectively reduce the local buckling near the impacted region. The comparison results of models M1–M5 show that the v_{cr} nonlinearly increased with the increase in α_c. The α_c interval between 0.25 and 0.75 was reduced to investigate the effect of α_c on v_{cr} in detail. FEA results demonstrates that the v_{cr} of the PCFST columns was significantly larger than that of the hollow steel tubular column (α_c=0) after concrete filling ($\alpha_c > 0$). For example, the critical impact velocities of models M1 and M4 were 3.65 and 10.95 m/s, respectively. For PCFST or CFST columns (α_c=0.25–1.0), the v_{cr} firstly decreased with α_c until α_c approached 0.5 and then increased as α_c continually increased. This finding indicates that the stress waves generated by impact load propagated to the interface of the concrete-filled and hollow steel tubular sections. The interface was near the mid-span for columns with α_c of 0.5 and also the weak zone of specimens. Thus, considerable deformations normally occurred at the interface, resulting in the reduced bearing capacity of columns.

Table 1. Numerical results of structural parameters

Label	α_c	R	f_{cu}(MPa)	Deformation mode	Δ_{max}(mm)	v_{cr}(m/s)
M1	0	46.7	30	G + L(F)	–	3.65
M2	0.25	46.7	30	G + L	18.65	6.95

M3	0.50	46.7	30	G + L	17.49	5.35
M4	0.75	46.7	30	G	16.85	10.95
M5	1.00	46.7	30	G	15.98	15.35
M6	0.47	70.0	30	G + L(F)	–	1.35
M7	0.47	56.0	30	G + L(F)	–	3.15
M8	0.47	46.7	30	G + L	17.78	5.35
M9	0.47	40.0	30	G	14.46	8.05
M10	0.47	35.0	30	G	12.96	10.85
M11	0.47	46.7	20	G + L	18.03	5.25
M12	0.47	46.7	30	G + L	17.78	5.35
M13	0.47	46.7	40	G + L	17.54	5.35
M14	0.47	46.7	50	G + L	17.50	5.55
M15	0.47	46.7	60	G + L	17.59	5.65

3.2.2 Width–thickness ratio of steel tube (*R*)

The influence of R on the impact response was analysed by changing the wall thickness of the steel tube from 2 to 4 mm at 0.5 mm intervals. Figure 4 (b) shows the effect of R on impact force–displacement (F–Δ) curve. From Figure 4 (b) and table 1, the local buckling near the interface and Δ_{max} decreased with the decrease in R, whereas the impact force and v_{cr} significantly increased. The results also show that R caused a significant effect on the anti-impact performance of the columns. The anti-impact performance of the columns increased with the decrease in R.

3.2.3 Concrete compressive strength (f_{cu})

The influence of f_{cu} on the impact response was analysed by changing f_{cu} from 20 MPa to 60 MPa at intervals of 10 MPa. Figures 4 (c) shows the effect of f_{cu} on the impact force–displacement (F–Δ) curve and v_{cr}. From Figure 4 (c) and table 1, the impact force, Δ_{max} and v_{cr} slightly changed with the increase in f_{cu}. The F–Δ curves in Figure 4 (c) almost overlapped. The results show that improving f_{cu} resulted in an insignificant effect on the anti-impact performance of columns.

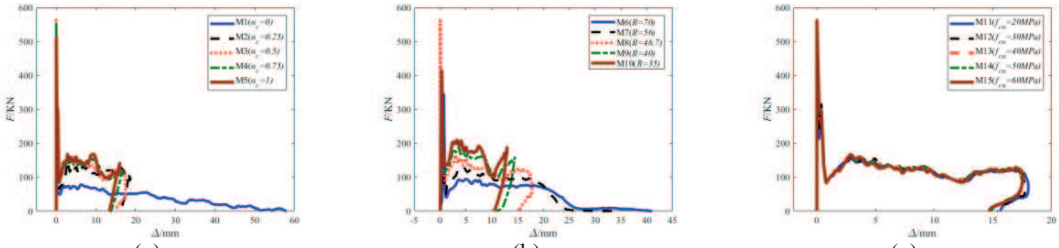

(a) (b) (c)

Figure 4. Impact force versus displacement time curve

3.3. Analysis of load parameters

The load parameters m, θ and μ were analysed. Table 2 lists the parameter settings and numerical results. The basic data of models M16–M30 are as follows: cross-section size $w_0 \times d_0 \times t$ = 140 mm × 80 mm × 3 mm, column height h = 1500 mm, concrete-filling height h_c = 700 mm, steel strength f_y = 345 MPa, concrete strength f_{cu} = 30 MPa and impact velocity v_0 = 4 m/s.

3.3.1 Impact mass (*m*)

The influence of m on the impact response was analysed by changing m from 200 kg to 600 kg at intervals of 100 kg. Figures 5 (a) shows the effect of m on the impact force–displacement (F–Δ) curve. From Figure 5 (a) and table 2, the impact energy and impulse increased with the increase in m, resulting in a significant increase in Δ_{max}. However, the impact force remained

constant with m. When the impact mass was small (m = 200 kg), the column would be destroyed only if the impact energy and v_{cr} were larger than models M17–M20. Moreover, when m ranged

Table 2. Numerical results of load parameters

Label	m(kg)	θ(°)	μ	Deformation mode	Δ_{max}(mm)	v_{cr}(m/s)
M16	**200**	90	0.3	G + L	13.14	7.25
M17	**300**	90	0.3	G + L	19.81	4.95
M18	**400**	90	0.3	G + L	28.94	4.15
M19	**500**	90	0.3	G + L(F)	–	3.75
M20	**600**	90	0.3	G + L(F)	–	3.35
M21	270	**75**	0.3	G + L	19.73	6.15
M22	270	**60**	0.3	G + L	18.42	7.05
M23	270	**45**	0.3	G + L	17.10	9.05
M24	270	**30**	0.3	G + L	15.75	12.35
M25	270	**15**	0.3	G + L	14.79	15.55
M26	270	90	**0.1**	G	16.75	16.35
M27	270	90	**0.2**	G + L	16.80	8.15
M28	270	90	**0.3**	G + L	17.78	5.35
M29	270	90	**0.4**	G + L(F)	–	3.75
M30	270	90	**0.5**	G + L(F)	–	2.65

from 300 kg to 600 kg, the v_{cr} difference was small, and the maximum difference was 8.4%. Therefore, a slight variation in v_{cr} occurred with the increase in m.

3.3.2 Impact angle (θ)

The influence of θ on the impact response was analysed by changing θ from 75° to 15° at 15° intervals. The impact position of models M21–M25 was the corner of a column. The line between the geometric centre of the rigid surface and the corner denotes the impact direction. The angle between the impact direction and x-axis was defined as θ. Figures 5 (b) shows the effect of θ on impact force–displacement (F–Δ) curve. From Figure 5 (b) and table 2, the angle between the impact direction and strong axis of the column continuously decreased with the decrease in θ. The deformation mode was dominated by global flexural deformation and local buckling near the impacted corner. The impact force F decreased with decreasing θ, whereas v_{cr} significantly increased. The results show that the local buckling under corner impact was larger than that under front impact. However, the column v_{cr} under front impact was smaller than that under corner impact.

3.3.3 Axial compression ratio (μ)

The influence of μ on the impact response was analysed by changing μ from 0.1 to 0.5 at intervals of 0.1. Figures 5 (c) shows the effect of μ on the impact force–displacement (F–Δ) curve. From figure 5 (c) and table 2, Δ_{max} gradually increased with the increase in μ, and the impact force presented a slight change. μ considerably influenced the impact response of the column. The larger the ratio, the lower the critical impact velocity the column could withstand.

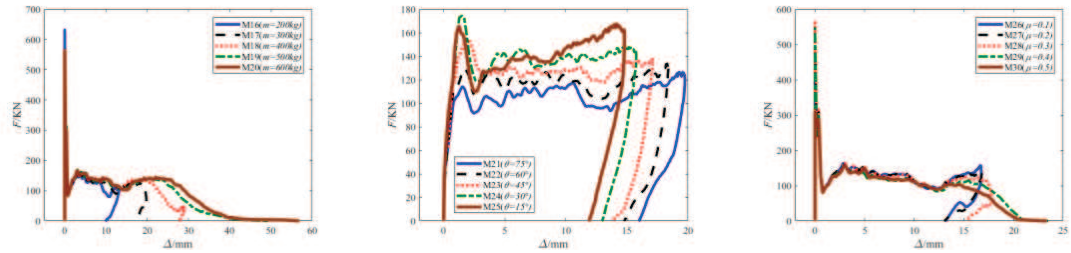

(a) (b) (c)

Figure 5. Impact force versus displacement time curve

4. Conclusion

This work conducted a numerical investigation on the anti-impact behaviour of the PCFST columns under static axial and lateral impact loads. Firstly, a finite element model was established. The element mesh, material properties, boundary conditions and contact were considered in this model. A static axial load was applied on the centre of the top end plate by a smooth step amplitude curve. The impact load was conducted at the height of 320 mm from the column bottom. Secondly, parameter analysis was carried out to further study the anti-impact behaviour. The numerical results could be summarised as follows. (1) The concrete-filling rate and width–thickness ratio of steel tube showed significant influence on the anti-impact performance of PCFST columns. Specially, when the concrete-filling rate was between 0.25 and 1.0, the critical impact velocity firstly decreased with the concrete-filling rate until the concrete-filling rate approached 0.5 and then increased as the concrete-filling rate continually increased. (2) Concrete compressive strength exhibited a significant influence on the anti-impact performance. The critical impact velocity and impact force–displacement curves slightly changed when the concrete compressive strength ranged from 20 MPa to 60 MPa. (3) The impact direction and axial compression ratio significantly affected the anti-impact performance of the PCFST columns. The critical impact velocity of the columns under corner impact direction was evidently larger than that under front impact direction. The critical impact velocity of the columns sharply decreased when the axial compression ratio increased. (4) The critical impact velocity slightly decreased with the increasing impact mass. Lastly, once the impact velocity reached the critical impact velocity, the columns would experience evident deformation and lose stability. Thus, important parameters, such as the concrete-filling rate, width–thickness ratio of steel tube, impact direction and axial compression ratio, should be considered in the design process.

Acknowledgement

The authors gratefully acknowledge the support of the National Natural Science Foundation of China (Nos. 51838006 and 51629801) and Fundamental Research Funds for the Central Universities (No. 2016YXMS095).

Reference

Abdelkarim O.I., Elgawady M.A., Performance of bridge piers under vehicle collision[J]. Engineering Structures, 2017, 140:337-352.

Abdel-Rahman N., Sivakumaran K.S., Material properties models for analysis of cold-formed steel members. Journal Structure Engineering, 1997, 123(9): 1135-1143.

Al-Thairy H., Wang Y., A numerical study of the behaviour and failure modes of axially compressed steel columns subjected to transverse impact. International Journal of Impact Engineering, 2011, 38: 732-744.

Baltay P., Gjelsvil A., Coefficient of friction for steel on concrete at high normal stress. Journal of Material in Civil Engineering 1990, 2(1): 46-49.